

Tetrahedral Interpolation on Regular Grids

Róbert Bán  and Gábor Valasek 

Eötvös Loránd University, Hungary
{rob.ban, valasek}@inf.elte.hu

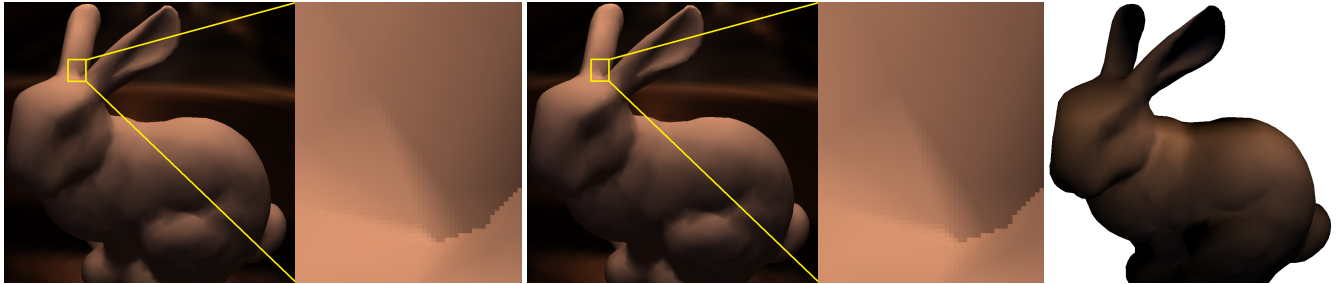


Figure 1: Comparison of trilinear (left) and tetrahedral (middle) interpolation between eight spatially fit second order spherical harmonics (SH) probes arranged in a cube around the Stanford bunny. The same region is zoomed in on left and center, to show the visual difference. The absolute difference image (right) is amplified 10-fold. Note how the contribution of the individual probes is different in the two methods, as further illustrated in Figure 3.

Abstract

This work proposes the use of barycentric interpolation on enclosing simplices of sample points to infer a reconstructed function from discrete data. In particular, we compare the results of trilinear and tetrahedral interpolation over regular 3D grids of second order spherical harmonics (SH) light probes. In general, tetrahedral interpolation only requires four data samples per query in contrast to the 8 samples necessary for trilinear interpolation, at the expense of a more expensive weight computation. Our tetrahedral implementation subdivides the cubical cells into six tetrahedra and uses the barycentric coordinates of the query position as weights to blend the probe data. We show that barycentric coordinates can be calculated efficiently in shaders for our particular tetrahedral decomposition of the cube, resulting only in simple arithmetic and conditional move operations.

CCS Concepts

• **Computing methodologies** → Rendering; Shape modeling; • **Mathematics of computing** → Continuous functions;

1. Introduction

In computer graphics, multivariate function representation are often represented as regular 3D grids of samples. There are several techniques to reconstruct a continuous function from the stored data. The standard method is trilinear interpolation that uses 8 samples and 7 linear interpolations to compute a filtered value.

An alternative approach is to subdivide the regular grid cells into tetrahedra and use the barycentric coordinates of the query position to weight the data of the vertices of the smallest enclosing tetrahedron. Kasson et al. [KPN93] proposed a similar solution for color conversion. The main advantage compared to trilinear interpolation is the reduced memory bandwidth. The contribution of our work is two-fold: (i) we propose to use the method in light probe interpolation and (ii) we present an efficient algorithm for the barycentric weight calculation.

2. Barycentric interpolation

Barycentric interpolation on an n -dimensional simplex is a linear combination of the vertices where the weights sum to 1. We can compare this to tensor interpolation which is defined on an n -cube as a tensor product of linear interpolations – also called bilinear and trilinear interpolation in 2 and 3 dimensions, respectively.

For barycentric interpolation, the cube is subdivided into a disjoint union of simplices. This subdivision is not unique. We decided to use the one shown in Figure 2 in 3D so that we can use a simplified barycentric weight computation algorithm (see Section 3).

Note that while barycentric and tensor interpolations yield different results, see Figure 3, one is not necessarily better than the other. Nevertheless, while both produce C^∞ reconstructed functions within their domains (i.e. tetrahedra and boxes), in general, the continuity of the inferred signal is only C^0 along the connections of these domains and a tetrahedral decomposition results in more of these boundaries.

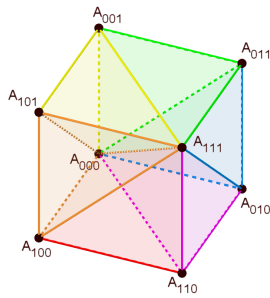


Figure 2: Cube decomposed into six congruent tetrahedra.

3. The algorithm

To compute the barycentric coordinates of a query point, first we have to identify which tetrahedron contains it, then compute the barycentric coordinates with respect to the vertices of that tetrahedron. The calculations are done in normalized cell coordinates ($\mathbf{x} = (x, y, z) \in [0, 1]^3$). The enclosing tetrahedron can be found by ordering the coordinates, since the six tetrahedra are (see Figure 2)

$$\begin{aligned} z \leq y \leq x, & & y \leq z < x, & & z < x \leq y, \\ x \leq z < y, & & y < x \leq z, & & x < y < z. \end{aligned} \quad (1)$$

Let us derive the weights for the first tetrahedron, highlighted with red in Figure 2. The vertices are A_{000} , A_{111} , A_{100} , and A_{110} , where the coordinates of A_{ijk} is $[i, j, k]^T \in \{0, 1\}^3$. The two equations defining the weights are

$$\begin{bmatrix} x \\ y \\ z \end{bmatrix} = w_0 \begin{bmatrix} 0 \\ 0 \\ 0 \end{bmatrix} + w_1 \begin{bmatrix} 1 \\ 1 \\ 1 \end{bmatrix} + w_2 \begin{bmatrix} 1 \\ 0 \\ 0 \end{bmatrix} + w_3 \begin{bmatrix} 1 \\ 1 \\ 0 \end{bmatrix}, \text{ and} \quad (2)$$

$$1 = w_0 + w_1 + w_2 + w_3. \quad (3)$$

The solution is $w_0 = 1 - x$, $w_1 = z$, $w_2 = x - y$, $w_3 = y - z$. The weights in the remaining five tetrahedra can be calculated similarly but we can write this more concisely. Let $a \leq b \leq c$, where $a = \min(x, y, z)$, $c = \max(x, y, z)$ and b the remaining coordinate. Then

$$w_0 = 1 - c, \quad w_1 = a, \quad w_2 = c - b, \quad w_3 = b - a. \quad (4)$$

The vertices are in a similar order: A_{000} and A_{111} are always the first two, w_2 corresponds to the remaining vertex closer to A_{000} and w_3 to the vertex closer to A_{111} .

Listing 1 shows our GLSL implementation. The function returns the barycentric weights and the 3D indices of the unknown vertices of the enclosing tetrahedron. The compiled code only uses conditional moves instead of branches, making it optimal for GPUs.

Listing 1: Barycentric calculation implementation in GLSL

```
void barycentricWeight(vec3 r, out vec4 bary,
                    out ivec3 vert2, out ivec3 vert3) {
    vert2 = ivec3(0,0,0); vert3 = ivec3(1,1,1);
    bvec3 c = greaterThanEqual(r.xyz, r.yzx);
    bool c_xy = c.x, c_yz = c.y, c_zx = c.z;
    bool c_yx = !c.x, c_zy = !c.y, c_xz = !c.z;
    bool cond; vec3 s;
#define ORDER(X,Y,Z) \
    cond = c_ ## X ## Y && c_ ## Y ## Z; \
    s = cond ? r.X ## Y ## Z : s; \
    vert2.X = cond ? 1 : vert2.X; \
```

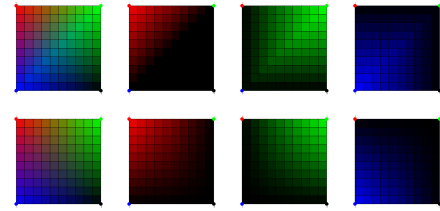


Figure 3: Comparison of barycentric (top row) and bilinear (bottom row) interpolation between four colors. The subfigures show the final result of the process (left column) as well as the individual contribution (i.e. color multiplied weight) of the top-left, top-right, and bottom-left data points in red, green, blue, respectively on the second to fourth columns.

```
vert3.Z = cond ? 0 : vert3.Z;
ORDER(x,y,z) ORDER(x,z,y) ORDER(z,x,y)
ORDER(z,y,x) ORDER(y,z,x) ORDER(y,x,z)
bary = vec4(1 - s.x, s.z, s.x - s.y, s.y - s.z);
}
```

4. Results

We compared trilinear and barycentric interpolation of light probes. Probes represent irradiance as second order SH functions containing $3 \times 9 = 27$ scalars. Figure 1 shows an example rendering of the Stanford bunny.

The table below compares nearest point sampling, manual trilinear interpolation, and tetrahedral interpolation of 2 million root searches on a 3D function represented by polynomials consisting of 1, 4, 10, and 20 scalars per sample in IEEE binary32 format, in 3D textures. The numbers are in milliseconds.

scalars per sample	AMD RX 5700				NVIDIA 2080			
	1	4	10	20	1	4	10	20
nearest	0.21	0.27	0.29	0.55	0.37	0.44	0.52	0.64
trilinear	0.73	0.99	2.30	4.42	0.50	0.79	1.40	2.37
tetrahedral	0.58	0.72	1.13	2.25	0.69	0.81	1.05	1.58

On both architectures, tetrahedral interpolation increases performance considerably for larger sample footprints. It even retains this gain compared to hardware accelerated trilinear interpolation from about 20 scalars per sample.

5. Conclusions

In summary, this work justifies the use of tetrahedral interpolation in probe light blending and provides an optimized algorithm for the weight calculations. We showed qualitative comparisons in 2D and 3D tests.

References

- [KPN93] KASSON J. M., PLOUFFE W., NIN S. I.: Tetrahedral interpolation technique for color space conversion. In *Device-Independent Color Imaging and Imaging Systems Integration* (1993), Motta R. J., Berberian H. A., (Eds.), vol. 1909, International Society for Optics and Photonics, SPIE, pp. 127 – 138. doi:10.1117/12.149035.1

Acknowledgement EFOP-3.6.3-VEKOP-16-2017-00001: Talent Management in Autonomous Vehicle Control Technologies – The Project is supported by the Hungarian Government and co-financed by the European Social Fund. Supported by the ÚNKP-20-3 New National Excellence Program of the Ministry for Innovation and Technology from the source of the National Research, Development and Innovation Fund. We would like to thank Visual Concepts for providing the AMD GPU used in the tests.